MNRAS **483,** L109–L113 (2019)
Advance Access publication 2018 November 30
doi:10.1093/mnrasl/sly226

A method to determine the evolution history of the mean neutral Hydrogen fraction

Rajesh Mondal [1]★ Somnath Bharadwaj,[2] Ilian T. Iliev [1] Kanan K. Datta,[3] Suman Majumdar [4,5] Abinash K. Shaw[2] and Anjan K. Sarkar[2]

[1]*Astronomy Centre, Department of Physics and Astronomy, University of Sussex, Falmer, Brighton BN19QH, UK*
[2]*Department of Physics and Centre for Theoretical Studies, Indian Institute of Technology Kharagpur, Kharagpur 721302, West Bengal, India*
[3]*Department of Physics, Presidency University, 86/1 College Street, Kolkata 700073, West Bengal, India*
[4]*Centre of Astronomy, Indian Institute of Technology Indore, Simrol, Indore 453552, Madhya Pradesh, India*
[5]*Department of Physics, Blackett Laboratory, Imperial College, Kensington, London SW7 2AZ, UK*

Accepted 2018 November 24. Received 2018 November 21; in original form 2018 October 16

ABSTRACT

The light-cone (LC) effect imprints the cosmological evolution of the redshifted 21-cm signal $T_{\rm b}(\hat{\boldsymbol{n}}, \nu)$ along the frequency axis that is the line-of-sight (LoS) direction of an observer. The effect is particularly pronounced during the epoch of reionization (EoR) when the mean hydrogen neutral fraction $\bar{x}_{\rm H\,I}(\nu)$ falls rapidly as the universe evolves. The multifrequency angular power spectrum $\mathcal{C}_\ell(\nu_1, \nu_2)$ quantifies the entire second-order statistics of $T_{\rm b}(\hat{\boldsymbol{n}}, \nu)$ considering both the systematic variation along ν due to the cosmological evolution and also the statistically homogeneous and isotropic fluctuations along all the three spatial directions encoded in $\hat{\boldsymbol{n}}$ and ν. Here, we propose a simple model where the systematic frequency (ν_1, ν_2) dependence of $\mathcal{C}_\ell(\nu_1, \nu_2)$ arises entirely due to the evolution of $\bar{x}_{\rm H\,I}(\nu)$. This provides a new method to observationally determine the reionization history. Considering an LC simulation of the EoR 21-cm signal, we use the diagonal elements $\nu_1 = \nu_2$ of $\mathcal{C}_\ell(\nu_1, \nu_2)$ to validate our model. We demonstrate that it is possible to recover the reionization history across the entire observational bandwidth provided we have the value $\bar{x}_{\rm H\,I}$ at a single frequency as an external input.

Key words: methods: statistical – dark ages, reionization, first stars – diffuse radiation – large-scale structure of Universe – cosmology: theory – observations.

1 INTRODUCTION

Observations of the redshifted 21-cm signal from neutral hydrogen (H I) are the most promising probe of the epoch of reionization (EoR). A considerable amount of effort is underway to detect the EoR 21-cm signal using ongoing and upcoming radio interferometric experiments, e.g. GMRT (Paciga et al. 2013), LOFAR (van Haarlem et al. 2013; Yatawatta et al. 2013), MWA (Bowman et al. 2013; Tingay et al. 2013; Dillon et al. 2014), PAPER (Parsons et al. 2014; Ali et al. 2015; Jacobs et al. 2015), SKA (Mellema et al. 2013; Koopmans et al. 2015), and HERA (DeBoer et al. 2017).

Using the redshifted H I 21-cm signal one can, in principle, map the H I distribution in the intergalactic medium in 3D with the line-of-sight (LoS) axis being the frequency (or redshift). However, an observer's view of the universe is restricted to the backward light cone (LC), and the H I 21-cm signal evolves along the LoS. This gives rise to the LC effect that has a significant impact on the EoR 21-cm signal and its various statistics. This has been taken into account by Barkana & Loeb (2006) and Zawada et al. (2014) while modelling the LC anisotropies in the two-point correlation function. Datta et al. (2012, 2014) and La Plante et al. (2014) have examined the impact of this effect on the EoR 21-cm 3D power spectrum, which is the primary observable of the first generation of radio interferometers.

Another important LoS effect is the redshift space distortion (RSD) due to the peculiar velocities of H I. Similar to the LC effect, RSD introduces anisotropies in the 21-cm signal (Bharadwaj & Ali 2004) along the LoS. Although, there has been substantial effort invested in including the RSD in EoR simulations by Mao et al. (2012), Majumdar, Bharadwaj & Choudhury (2013), Majumdar et al. (2016), and Jensen et al. (2013), the problem of how to properly include the peculiar velocities of H I in LC simulation was addressed by Mondal, Bharadwaj & Datta (2018).

The statistical homogeneity (or ergodicity) along the LoS gets destroyed by the LC effect. One of the main problems regarding the interpretation of the EoR 21-cm signal through its 3D power spec-

★ E-mail: Rajesh.Mondal@sussex.ac.uk

trum $P(\boldsymbol{k})$ lies in the signal's non-ergodic nature. The 3D power spectrum $P(\boldsymbol{k})$ assumes that the signal is ergodic and periodic, thus it provides a biased estimate of the statistics of EoR signal (Trott 2016). In contrast, the multifrequency angular power spectrum (hereafter MAPS) $\mathcal{C}_\ell(\nu_1, \nu_2)$ (Datta, Choudhury & Bharadwaj 2007) does not have any such intrinsic assumption in its definition. Mondal et al. (2018) have demonstrated that the entire second-order statistics of the non-ergodic LC EoR signal can be expressed by the MAPS.

In this letter, we demonstrate, as a proof of concept, how one can use the intrinsic non-ergodicity of the LC EoR 21-cm signal to uncover the underlying reionization history. The reionization history is one of the most sought-after outcomes of any experiment aiming to observe the EoR. We propose and validate a formalism whereby the measured MAPS can be used to extract the reionization history in a model-independent manner. In this letter, we have used the Planck+WP best-fitting values of cosmological parameters (Planck Collaboration XVI 2014).

2 SIMULATING THE LC 21-CM SIGNAL FROM THE EOR

In this section, we briefly summarize the simulation technique used for generating the LC EoR 21-cm signal. The reader is referred to section 2 of Mondal et al. (2018) for a detailed description of the simulations. Here, we have considered a region that spans the comoving distance range $r_{\rm n} = 9001.45$ Mpc (nearest) to $r_{\rm f} = 9301.61$ Mpc (farthest), which corresponds to the frequencies $\nu_{\rm n} = 166.91$ MHz and $\nu_{\rm f} = 149.04$ MHz, respectively. We have simulated snapshots of the H I distribution (*coeval* cubes) at 25 different comoving distances $r_{\rm i}$ in the aforesaid r range (see fig. 2 of Mondal et al. 2018), which were chosen so that the mean neutral Hydrogen fraction $\bar{x}_{\rm H\,I}$ varies approximately by an equal amount in each interval.

We have used seminumerical simulations to generate the coeval ionization cubes with a comoving volume $V = [300.16\,{\rm Mpc}]^3$. These simulations involve three main steps. First step involves a particle-mesh N-body code to simulate the dark matter distribution. The N-body run has 4288^3 grids with 0.07 Mpc grid spacing using 2144^3 dark matter particles (particle mass $1.09 \times 10^8\,{\rm M}_\odot$). In the next step, a Friends-of-Friends (FoF) algorithm is used to identify collapsed halos in the dark matter distribution. A fixed linking length of 0.2 times the mean inter-particle distance is used for the FoF and we have set the criterion that a halo should have at least 10 dark matter particles. In the third and last step, an ionization field is produced following an excursion set formalism (Furlanetto, Zaldarriaga & Hernquist 2004). For this, we have adopted the ionization parameters $\{N_{\rm ion},\ M_{\rm halo,min},\ R_{\rm mfp}\} = \{23.21,\ 1.09 \times 10^9\,{\rm M}_\odot,\ 20\,{\rm Mpc}\}$, identical to Mondal, Bharadwaj & Majumdar (2017). This final step closely follows the assumption of homogeneous recombination adopted by Choudhury, Haehnelt & Regan (2009). The H I distributions in our simulations are represented by particles whose H I masses were calculated from the neutral Hydrogen fraction $x_{\rm H\,I}$ interpolated from its eight adjacent grid points. The positions, peculiar velocities, and H I masses of these particles are then saved for each such coeval cube.

To construct the LC map, we slice the coeval maps at 25 different radial distances $r_{\rm i}$, and construct the LC map for the region between $r_{\rm i}$ and $r_{\rm i+1}$ with the H I particles from corresponding slices of the coeval snapshot. Finally, we map the H I particles within the LC box from $\boldsymbol{r} = r\hat{\boldsymbol{n}}$ to observing frequency ν and direction $\hat{\boldsymbol{n}}$, which are the appropriate variables for the observations of redshifted 21-cm brightness temperature fluctuations $\delta T_{\rm b}(\hat{\boldsymbol{n}},\ \nu)$ in 3D. Note that for this mapping, the cosmological expansion and the radial component of the H I peculiar velocity $\hat{\boldsymbol{n}} \cdot \boldsymbol{v}$ together determine the observed frequency ν for the 21-cm signal originating from the point $\hat{\boldsymbol{n}}r$. Our LC box is centred at the comoving distance $r_{\rm c} = 9151.53$ Mpc ($\nu_{\rm c} = 157.78$ MHz), which corresponds to the redshift $\approx$8. The mass-averaged H I fraction $\bar{x}_{\rm H\,I}$ at the centre of the LC simulation is $\approx$0.51, and it changes from $\bar{x}_{\rm H\,I} \approx 0.65$ (at farthest end) to $\bar{x}_{\rm H\,I} \approx 0.35$ (at nearest end), following the reionization history of Mondal et al. (2018).

3 MODELLING THE MULTIFREQUENCY ANGULAR POWER SPECTRUM

The issue under consideration here is 'How to quantify the statistics of the non-ergodic EoR 21-cm signal $\delta T_{\rm b}(\hat{\boldsymbol{n}},\ \nu)$ in 3D?'. We know that the LC effect makes the cosmological 21-cm signal ($\delta T_{\rm b}(\hat{\boldsymbol{n}},\ \nu)$) evolve significantly along the LoS direction ν. The 3D power spectrum $P(\boldsymbol{k})$ is not accurate when the statistical properties of the signal evolve along a specific direction. Additionally, the Fourier transform imposes periodicity on the signal, an assumption that cannot be justified along the LoS when the LC effect has been taken into account. As a consequence, the 3D power spectrum fails to quantify the entire information in the signal and gives a biased estimate of the statistics (Trott 2016; Mondal et al. 2018). In contrast to this the MAPS $\mathcal{C}_\ell(\nu_1, \nu_2)$ quantifies the entire second-order statistics of the EoR 21-cm signal even in the presence of the LC effect (Mondal et al. 2018).

The redshifted 21-cm brightness temperature fluctuations are decomposed into spherical harmonics as

$$\delta T_{\rm b}(\hat{\boldsymbol{n}},\ \nu) = \sum_{\ell,m} a_{\ell{\rm m}}(\nu)\, Y_\ell^{\rm m}(\hat{\boldsymbol{n}})\,, \tag{1}$$

and these are used to define the MAPS (Datta et al. 2007) using

$$\mathcal{C}_\ell(\nu_1, \nu_2) = \left\langle a_{\ell{\rm m}}(\nu_1)\, a^*_{\ell{\rm m}}(\nu_2) \right\rangle . \tag{2}$$

This takes into account the assumption that the EoR 21-cm signal is statistically homogeneous and isotropic with respect to different directions in the sky; however, it does not assume the signal to be statistically homogeneous along the LoS direction ν. Considering the particular situation where the signal is ergodic (statistically homogeneous) along the LoS, we have $\mathcal{C}_\ell(\nu_1, \nu_2) = \mathcal{C}_\ell(\Delta\nu)$, *i.e.* it depends only on the frequency separation $\Delta\nu = \|\nu_1 - \nu_2\|$.

Under the assumption that the H I spin temperature is much larger than the CMB temperature, i.e. $T_{\rm s} \gg T_\gamma$, the redshifted 21-cm brightness temperature fluctuations (equations 4 and A5 of Bharadwaj & Ali 2005) can be expressed as (Mondal et al. 2018)

$$T_{\rm b}(\hat{\boldsymbol{n}}, \nu) = \bar{T}_0\, \frac{\rho_{\rm H\,I}}{\bar{\rho}_{\rm H}} \left(\frac{H_0 \nu_{\rm e}}{c}\right) \left|\frac{\partial r}{\partial \nu}\right|, \tag{3}$$

where

$$\bar{T}_0 = 4.0\,{\rm mK} \left(\frac{\Omega_{\rm b} h^2}{0.02}\right) \left(\frac{0.7}{h}\right), \tag{4}$$

$\rho_{\rm H\,I}/\bar{\rho}_{\rm H}$ is the ratio of the neutral hydrogen density to the mean hydrogen density, and r refers to the comoving distance from which the redshifted H I emission, observed at frequency ν, is originated. The factors $\rho_{\rm H\,I}/\bar{\rho}_{\rm H}$ and $\partial r/\partial \nu$ both evolve along the LoS direction (ν or z) due to a variety of factors including the evolution of various quantities pertaining to the background cosmological model and the growth of density perturbation in $\rho_{\rm H\,I}$. However, during the EoR the evolution of the mean mass-weighted neutral hydrogen fraction $\bar{x}_{\rm H\,I} = \bar{\rho}_{\rm H\,I}/\bar{\rho}_{\rm H}$ by far dominates over the other factors

that cause $T_{\rm b}(\hat{\boldsymbol{n}}, \nu)$ to evolve along the LoS direction. Based on this, we propose a model

$$\mathcal{C}_\ell(\nu_1, \nu_2) = \bar{x}_{\rm H\,I}(\nu_1)\, \bar{x}_{\rm H\,I}(\nu_2)\, \mathcal{C}_\ell^{\rm E}(\Delta\nu)\,, \tag{5}$$

where $\mathcal{C}_\ell^{\rm E}(\Delta\nu)$ is ergodic along the LoS, and the factor $\bar{x}_{\rm H\,I}(\nu_1)\, \bar{x}_{\rm H\,I}(\nu_2)$ that accounts for the evolution of the mean hydrogen neutral fraction breaks the ergodicity along the LoS. We expect the above relation to hold at small scales where the H I density traces the underlying DM density. However, at scales larger than the typical bubble size the evolution is expected to be dominated by the evolution of bubble sizes and the above relation may not stay valid in that regime. This will provide a handle to measure the evolution of the H I neutral fraction $\bar{x}_{\rm H\,I}(z)$ as reionization proceeds. Unfortunately, this will only allow us to determine the ratio $\bar{x}_{\rm H\,I}(z_2)/\bar{x}_{\rm H\,I}(z_1)$ at two different epochs, and it will not allow us to uniquely determine $\bar{x}_{\rm H\,I}(z_1)$ or $\bar{x}_{\rm H\,I}(z_2)$. For the purpose of this letter, we consider

$$\frac{\bar{x}_{\rm H\,I}(z_2)}{\bar{x}_{\rm H\,I}(z_1)} = \sqrt{\frac{\mathcal{C}_\ell(\nu_2, \nu_2)}{\mathcal{C}_\ell(\nu_1, \nu_1)}}\,, \tag{6}$$

which does not uniquely determine the H I reionization history. However, the reionization history is uniquely specified if we combine these measurements with a single measurement of $\bar{x}_{\rm H\,I}$ at any particular epoch say z_1 using an independent method (e.g. Majumdar, Bharadwaj & Choudhury 2012).

4 VALIDATING OUR MODEL

As a first step towards validating our model, we consider a situation where the brightness temperature fluctuations are, by construction, of the form

$$\delta T_{\rm b}(\hat{\boldsymbol{n}}, \nu) = f(\nu) \times \delta_{\rm e}(\hat{\boldsymbol{n}}, \nu)\,, \tag{7}$$

where $f(\nu)$ is a known function and $\delta_{\rm e}(\hat{\boldsymbol{n}}, \nu)$ is a random field that is isotropic in $\hat{\boldsymbol{n}}$ and ergodic in ν. Using this, we investigate whether our method of analysis can determine $f(\nu)$ from the estimated $\mathcal{C}_\ell(\nu_1, \nu_2)$. Here, we have simulated 10 000 statistically independent realizations of homogeneous and isotropic Gaussian random fields $\delta_{\rm e}(\boldsymbol{x})$ corresponding to a realization of the CDM power spectrum $P_{\rm DM}(k)$. Working in the regime where the flat-sky approximation holds true, we have converted the comoving displacement with respect to the centre of the box $\boldsymbol{x} = (\boldsymbol{x}_\perp, x_\parallel)$ to angle and frequency, respectively, using $\boldsymbol{\theta} = \boldsymbol{x}_\perp/r$ and $\nu - \nu_{\rm c} = x_\parallel/r'$ where we assume that the centre of the simulation box is located at a redshift $z_{\rm c} = 1420\,{\rm MHz}/\nu_{\rm c}$ with corresponding comoving distance r and with $r' = {\rm d}r/{\rm d}\nu$ evaluated at $\nu_{\rm c}$. The resulting $\delta_{\rm e}(\boldsymbol{\theta}, \nu)$ is statistically isotropic in $\boldsymbol{\theta}$ and ergodic in ν. The ergodicity along the LoS is broken by the function $f(\nu)$, which we have assumed to be of the form

$$f(\nu) = 1 - a\left(\frac{\nu - \nu_{\rm c}}{B}\right)\,. \tag{8}$$

Here, $f(\nu)$ is a linear function that has a value $f(\nu_{\rm c}) = 1$ at the centre of the frequency bandwidth B, and it has values $f = 1 - a/2$ and $f = 1 + a/2$ at the nearest and farthest edges of the band, respectively. In principle, one can choose different forms of $f(\nu)$. The aim here is to mimic a situation where we are analysing observations of a part of the reionization history where the evolution of the neutral fraction is approximately linear (see fig. 2 of Mondal et al. 2018). Different values of a correspond to different values of the slope or equivalently different values of the reionization rate. The different panels of Fig. 1 show $\delta T_{\rm b}(\boldsymbol{\theta}, \nu)$ for a single realization of $\delta_{\rm e}(\boldsymbol{x})$ considering different values of a.

We have used the simulated $\delta T_{\rm b}(\boldsymbol{\theta}, \nu)$ to estimate $\mathcal{C}_\ell(\nu_1, \nu_2)$ in the flat-sky approximation (Mondal et al. 2018). Here, we focus on the diagonal elements $\nu_1 = \nu_2$ where the MAPS signal peaks. In principle, one can use the full information contained in MAPS matrix $\mathcal{C}_\ell(\nu_1, \nu_2)$ to analyse the results. However, for simplicity we have only considered the diagonal terms. We have used the ratio $A\sqrt{\mathcal{C}_\ell(\nu)/\bar{\mathcal{C}}_\ell}$ to determine $f(\nu)$ from our simulations. Here, $\mathcal{C}_\ell(\nu) \equiv \mathcal{C}_\ell(\nu, \nu)$, $\bar{\mathcal{C}}_\ell = B^{-1}\int_{-B/2}^{B/2} \mathcal{C}_\ell(\nu)\,{\rm d}\nu$, and A is a normalization constant whose value has to be externally specified. Here, we use the prior information that $f(\nu_{\rm c}) = 1$ to decide the value of A. Fig. 2 shows the ratio $A\sqrt{\mathcal{C}_\ell(\nu)/\bar{\mathcal{C}}_\ell}$ evaluated at different ℓ values, which all have been shown as a function of $\nu - \nu_{\rm c}$. We have used 10 equally spaced logarithmic ℓ bins. We find that the ratio is independent of ℓ, i.e. they all overlap. We also see that the ratio is able to correctly recover the functional form $f(\nu)$ from the simulations shown in Fig. 1. This validates our method of analysis.

We next apply the same method to our LC simulations to test if our model (equation 5) actually holds for the simulated EoR 21-cm signal. The LC EoR 21-cm signal is undoubtedly non-ergodic along the LoS. An earlier work (fig. 9 of Mondal et al. 2018) demonstrates that $\mathcal{C}_\ell(\nu)/\bar{\mathcal{C}}_\ell - 1$ shows a systematic variation with ν, the value of $\mathcal{C}_\ell(\nu)/\bar{\mathcal{C}}_\ell - 1$ is found to increase as we move from the nearest to the farthest end of the simulation box along LoS. This result correlates well with the fact that $\bar{x}_{\rm H\,I}$ increases along the LoS direction. This systematic variation, however, is only seen at the large ℓ bins (small angular scales) where we have a large number of Fourier modes in each bin. This systematic variation is not seen in the small ℓ bins, partly because of the fewer number of Fourier modes in each bin (leading to a large sample variance) and partly due to the fact that the evolution of the H I signal at these scales is dominated by the evolution of ionized bubbles not the $\bar{x}_{\rm H\,I}$. To avoid this uncertainty, we restrict the ℓ range to $\ell > 2571$ for the present analysis.

We divide the ℓ range corresponding to our LC simulation into equally spaced logarithmic bins, and we compute $\sqrt{\mathcal{C}_\ell(\nu)/\bar{\mathcal{C}}_\ell}$ for all of these bins for which $\ell > 2571$. We see that the values of $\sqrt{\mathcal{C}_\ell(\nu)/\bar{\mathcal{C}}_\ell}$ display a large scatter (Fig. 3), *i.e.* for a fixed ν we find a range of values of $\sqrt{\mathcal{C}_\ell(\nu)/\bar{\mathcal{C}}_\ell}$ across the different ℓ bins. We attempt to mitigate the effect of these variations by estimating $\mathcal{C}(\nu)$ that is obtained by combining the signal in all the modes with $\ell > 2571$ into a single bin. Note that the EoR 21-cm signal is highly non-Gaussian (Bharadwaj & Pandey 2005; Mondal et al. 2015; Majumdar et al. 2018), which makes it quite non-trivial to predict errors for the estimated $\mathcal{C}(\nu)$ (Mondal, Bharadwaj & Majumdar 2016), and we have not attempted this here. Apart from the cosmic variance there will be instrumental noise, which will further worsen our predictions (i.e. the goodness of fit χ^2 of our model).

We find that in addition to a systematic increase with decreasing frequency, the values of $\sqrt{\mathcal{C}(\nu)/\bar{\mathcal{C}}}$ exhibit an apparently random fluctuation with varying frequency (Fig. 3). In order to model this systematic variation, we have fitted a second-order polynomial $\sqrt{\mathcal{C}(\nu)/\bar{\mathcal{C}}} = a_0 + a_1\left(\frac{\nu-\nu_{\rm c}}{B}\right) + a_2\left(\frac{\nu-\nu_{\rm c}}{B}\right)^2$ to the values estimated from the LC simulation. We have used a least-squares fit to obtain the best-fitting a_0, a_1, and a_2. We find that the best-fitting curve captures the systematic variation of $\sqrt{\mathcal{C}(\nu)/\bar{\mathcal{C}}}$ quite well and the residuals after subtracting out the fit appear to be consistent with random fluctuations around zero (the lower panel of Fig. 3). If our model (equation 5) holds, we then have $\bar{x}_{\rm H\,I}(\nu) = A\sqrt{\mathcal{C}(\nu)/\bar{\mathcal{C}}}$. As mentioned earlier, it is necessary to introduce one additional input to determine the value of A. Here, we use the information that we

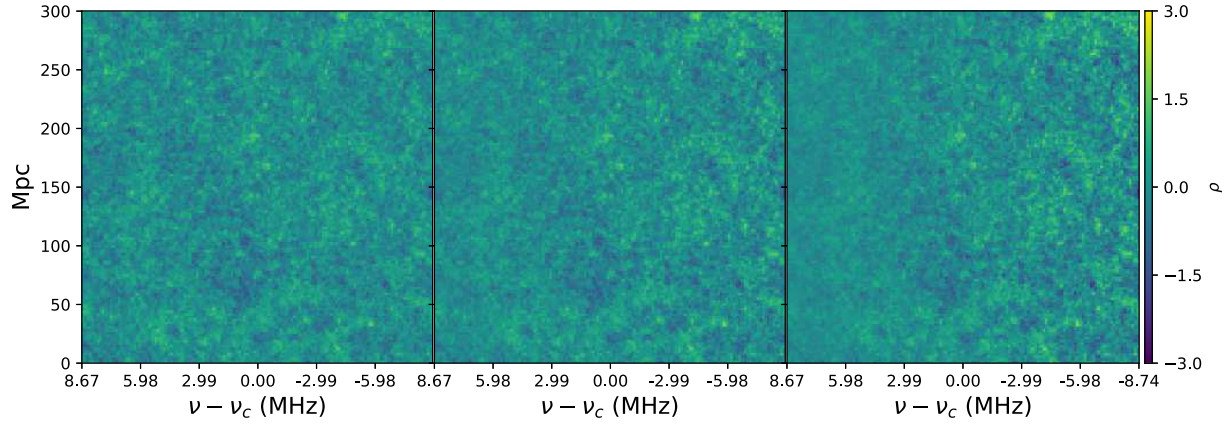

Figure 1. This shows a section through one realization of the different Gaussian brightness temperature fluctuation fields for $a = 0$ (ergodic), 0.5, and 1.0 (see equation 8). In the panels, the value of a increases from the left to the right.

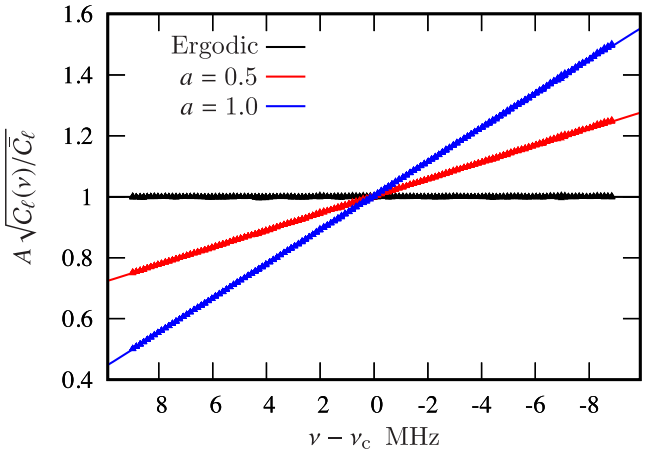

Figure 2. This shows $A\sqrt{\mathcal{C}_\ell(\nu)/\bar{\mathcal{C}}_\ell}$ for different values of a as shown in the figure. The points show results from our simulations and the solid lines show the function $f(\nu)$ (equation 8).

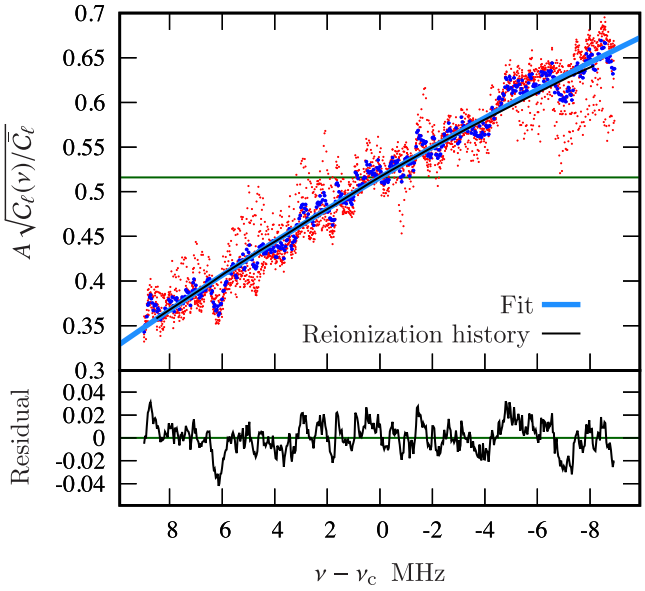

Figure 3. The upper panel shows $A\sqrt{\mathcal{C}_\ell(\nu)/\bar{\mathcal{C}}_\ell}$ estimated from our LC EoR simulation. The red points show the results at different ℓ bins with $\ell > 2571$. The blue points show $A\sqrt{\mathcal{C}(\nu)/\bar{\mathcal{C}}}$, which have been estimated by combining all the modes with $\ell > 2571$ into a single bin. The light blue solid line shows the second-order polynomial fit to the values of $A\sqrt{\mathcal{C}(\nu)/\bar{\mathcal{C}}}$ and the lower panel shows the residual after subtracting out the fit. The black solid line shows the values of $\bar{x}_{\rm H\,I}(\nu)$ corresponding to the reionization history of our LC simulation. The horizontal green line shows the value $\bar{x}_{\rm H\,I}(\nu_c) = 0.51$.

have $\bar{x}_{\rm H\,I} \approx 0.51$ at $\nu_c = 157.78$ MHz. We use this in conjunction with the polynomial fit to determine the value of A. Fig. 3 shows a comparison of $\bar{x}_{\rm H\,I}(\nu)$ corresponding to the reionization history (see fig. 2 of Mondal et al. 2018) of our LC simulation and the best-fitting values of $A\sqrt{\mathcal{C}(\nu)/\bar{\mathcal{C}}}$ estimated from the LC simulation. We find that the two are in close agreement, thereby validating our model.

5 SUMMARY AND CONCLUSIONS

The LC effect imprints the cosmological evolution history on the redshifted H I 21-cm signal $T_{\rm b}(\hat{\boldsymbol{n}}, \nu)$ along the LoS direction ν. This effect is particularly pronounced during EoR when $\bar{x}_{\rm H\,I}(\nu)$ falls rapidly as the universe evolves. The MAPS $\mathcal{C}_\ell(\nu_1, \nu_2)$ fully quantifies the second-order statistics of $T_{\rm b}(\hat{\boldsymbol{n}}, \nu)$. It does not assume the signal to be ergodic along the LoS direction ν, and the frequency (ν_1, ν_2) dependence of $\mathcal{C}_\ell(\nu_1, \nu_2)$ quantifies both the systematic variation and the random fluctuations of the signal along ν. Here, we have proposed a simple model (equation 5) where the systematic variations of $\mathcal{C}_\ell(\nu_1, \nu_2)$ with (ν_1, ν_2) arise entirely due to the evolution of $\bar{x}_{\rm H\,I}(\nu)$. This provides a unique method to observationally determine the reionization history of the universe.

In this letter, we have used an LC simulation of the EoR 21-cm signal to estimate $\mathcal{C}_\ell(\nu_1, \nu_2)$. Using the diagonal elements $\mathcal{C}_\ell(\nu) \equiv \mathcal{C}_\ell(\nu, \nu)$, we show that our model (equation 5) is indeed valid for large values of ℓ. Assuming an external input, which provides us with the value of $\bar{x}_{\rm H\,I}(\nu_c)$ at a particular frequency ν_c, we demonstrate that it is possible to recover the reionization history $\bar{x}_{\rm H\,I}(\nu)$ from the estimated $\mathcal{C}_\ell(\nu)$ across the entire observational bandwidth B. The accuracy of our estimates depends on how accurately the value of $\bar{x}_{\rm H\,I}$ is measured at a particular frequency. An incorrect determination of $\bar{x}_{\rm H\,I}$ will result in a biased estimate of the reionization history.

The present analysis of $\mathcal{C}_\ell(\nu_1, \nu_2)$ is restricted to the diagonal elements $(\nu_1 = \nu_2)$. The analysis can be enlarged to include the information contained in the non-diagonal elements and thereby

improve the signal-to-noise ratio for the recovered $\bar{x}_{\rm H\,I}(\nu)$. It is however necessary to note that the EoR 21-cm signal is largely localized in the elements within the vicinity of the diagonal elements, and the elements at a large frequency separation $\|\nu_1 - \nu_2\|$ do not contain significant signal (Bharadwaj & Ali 2005; Datta et al. 2007). We plan to address these issues in a future work.

Our analysis is a proof of concept and based on simple seminumerical simulations. The details will possibly differ if one uses high-resolution simulations or includes fully coupled 3D radiative transfer (e.g. Iliev et al. 2006; Gnedin, Becker & Fan 2017). However, one can treat our predictions as being characteristic of the qualitative nature of the non-ergodic LC EoR 21-cm signal.

ACKNOWLEDGEMENTS

This work was supported by the Science and Technology Facilities Council (grant numbers ST/F002858/1 and ST/I000976/1) and the Southeast Physics Network (SEPNet).

REFERENCES

Ali Z. S. et al., 2015, ApJ, 809, 61
Barkana R., Loeb A., 2006, MNRAS, 372, L43
Bharadwaj S., Ali S. S., 2004, MNRAS, 352, 142
Bharadwaj S., Ali S. S., 2005, MNRAS, 356, 1519
Bharadwaj S., Pandey S. K., 2005, MNRAS, 358, 968
Bowman J. D. et al., 2013, PASA, 30, e031
Choudhury T. R., Haehnelt M. G., Regan J., 2009, MNRAS, 394, 960
Datta K. K., Choudhury T. R., Bharadwaj S., 2007, MNRAS, 378, 119
Datta K. K., Mellema G., Mao Y., Iliev I. T., Shapiro P. R., Ahn K., 2012, MNRAS, 424, 1877
Datta K. K., Jensen H., Majumdar S., Mellema G., Iliev I. T., Mao Y., Shapiro P. R., Ahn K., 2014, MNRAS, 442, 1491
DeBoer D. R. et al., 2017, PASP, 129, 045001
Dillon J. S. et al., 2014, Phys. Rev. D, 89, 023002
Furlanetto S. R., Zaldarriaga M., Hernquist L., 2004, ApJ, 613, 16
Gnedin N. Y., Becker G. D., Fan X., 2017, ApJ, 841, 26
Iliev I. T., Mellema G., Pen U.-L., Merz H., Shapiro P. R., Alvarez M. A., 2006, MNRAS, 369, 1625
Jacobs D. C. et al., 2015, ApJ, 801, 51
Jensen H. et al., 2013, MNRAS, 435, 460
Koopmans L. et al., 2015, Proc. Sci., The Cosmic Dawn and Epoch of Reionisation with SKA. SISSA, Trieste, POS#001, available at: http://adsabs.harvard.edu/abs/2015aska.confE...1K
La Plante P., Battaglia N., Natarajan A., Peterson J. B., Trac H., Cen R., Loeb A., 2014, ApJ, 789, 31
Majumdar S. et al., 2016, MNRAS, 456, 2080
Majumdar S., Bharadwaj S., Choudhury T. R., 2012, MNRAS, 426, 3178
Majumdar S., Bharadwaj S., Choudhury T. R., 2013, MNRAS, 434, 1978
Majumdar S., Pritchard J. R., Mondal R., Watkinson C. A., Bharadwaj S., Mellema G., 2018, MNRAS, 476, 4007
Mao Y., Shapiro P. R., Mellema G., Iliev I. T., Koda J., Ahn K., 2012, MNRAS, 422, 926
Mellema G. et al., 2013, Exp. Astron., 36, 235
Mondal R., Bharadwaj S., Majumdar S., Bera A., Acharyya A., 2015, MNRAS, 449, L41
Mondal R., Bharadwaj S., Majumdar S., 2016, MNRAS, 456, 1936
Mondal R., Bharadwaj S., Majumdar S., 2017, MNRAS, 464, 2992
Mondal R., Bharadwaj S., Datta K. K., 2018, MNRAS, 474, 1390
Paciga G. et al., 2013, MNRAS, 433, 639
Parsons A. R. et al., 2014, ApJ, 788, 106
Planck Collaboration XVI, 2014, A&A, 571, A16
Tingay S. J. et al., 2013, PASA, 30, e007
Trott C. M., 2016, MNRAS, 461, 126
van Haarlem M. P. et al., 2013, A&A, 556, A2
Yatawatta S. et al., 2013, A&A, 550, A136
Zawada K., Semelin B., Vonlanthen P., Baek S., Revaz Y., 2014, MNRAS, 439, 1615

This paper has been typeset from a TEX/LATEX file prepared by the author.